Application of Magnetically-Broadened Hydrogenic Line Profiles to Computational Modeling of a Plasma Experiment

M.L. Adams, H.A. Scott, R.W. Lee, J.L. Terry,
E.S. Marmar, B. Lipschultz, A.Yu. Pigarov, J.P. Freidberg

December 2000

Plasma Science and Fusion Center
Massachusetts Institute of Technology
Cambridge, MA 02139, USA

Application of Magnetically-Broadened Hydrogenic Line Profiles to Computational Modeling of a Plasma Experiment

M.L. Adams [a],[*]   H.A. Scott, [b] R.W. Lee, [b] J.L. Terry, [c]
E.S. Marmar, [c] B. Lipschultz, [c] A.Yu. Pigarov, [d] J.P. Freidberg [a]

[a]*MIT, NW16, 167 Albany St., Cambridge, MA 02139, USA*

[b]*LLNL, University of California, P.O. Box 808, Livermore, CA 94550, USA*

[c]*MIT, NW17, 175 Albany St., Cambridge, MA 02139, USA*

[d]*UCSD, 474 Engineering Building II, La Jolla, CA 92093, USA*

Abstract

Magnetically-broadened hydrogenic line profiles are used, in conjunction with a non-local thermodynamic equilibrium (NLTE) code, to model an optically thick phenomenon in the Alcator C-Mod tokamak fusion experiment. The line profiles, including magnetic field effects as well as Doppler and Stark broadening, have been calculated using Beline and are used in Cretin, a multi-dimensional NLTE radiation transfer code, to study the influence of a magnetic field on emergent spectrum. A midplane Alcator C-Mod MARFE (Multifaceted Axisymmetric Radiation From the Edge), in which the magnetic field strength was changed dynamically from 5.4T down to 2.7T, is simulated and compared with experimental data. Assuming hydrodynamic and radiative equilibrium, MARFE simulations are performed in one-dimension with fixed plasma density and temperature profiles. Magnetic broadening effects on the brightness of optically thick Lyman series lines are quantified.

Key words: magnetic field, numerical, plasma diagnostics, radiation transport

1   Introduction

In order to design tokamak divertors, and hence optimize power handling, radiation transport must be considered. Experiments studying edge plasma

* TEL: 001-617-258-7525; FAX: 001-617-253-5805
  Email address: adams@mit.edu (M.L. Adams).

recombination on the Alcator C-Mod tokamak have shown that several Lyman series hydrogenic lines are optically thick.[1] Since the flow of radiation energy in these plasmas is dominated by line radiation, accurate line profile calculations are important to tokamak divertor design. This paper investigates the application of magnetically-broadened hydrogenic line profiles to the computational modeling of radiation emerging from the magnetic fusion experiment (MFE) Alcator C-Mod.

Although theoretical details of magnetically-broadened hydrogenic line profiles have been published elsewhere [2,3], it is advantageous to review the salient ingredients of the present model to both assist in our understanding of the spectroscopic applications and motivate future improvements. The code Beline [3] calculates line profiles including magnetic field effects, as well as Stark and Doppler broadening. The line profiles exhibit the quantum mechanical energy levels of a hydrogenic atom in the combined presence of an external magnetic field and internal ion electric plasma microfield. Broadening of allowed transitions between bound states is calculated assuming a Maxwellian velocity distribution of emitters, and using various binary electron collision models. Each of these theoretical elements is directly observable and may be exploited to obtain useful plasma diagnostic information, provided the region of line radiation emission is localized in position space and the emitted photons have a low probability of scattering. These conditions are not always satisfied and a more general analysis of line radiation features for diagnostic purposes, especially those pertaining to the magnetic field, is needed.

The Balmer lines in Alcator C-Mod are optically thin. For a spatially localized radiation phenomenon, such as a MARFE (Multifaceted Axisymmetric Radiation From the Edge) [4], spectroscopic analysis of Balmer radiation provides a simple diagnostic for the emission region. We refer to this as a "local" analysis to signify that only properties of a localized region of the plasma are involved.

Local line profile analysis is a useful diagnostic tool, but it is not valid for optically thick lines or emission regions with large gradients. Furthermore, this analysis does not provide useful information regarding the flow of radiation energy. In Alcator C-Mod several of the Lyman lines are optically thick, and the full plasma system must be considered to determine plasma properties. To model the experimental spectral measurements of the Lyman series, we perform numerical calculations that self-consistently solve the full atomic kinetics and radiation transfer equations using appropriate line profiles in the code Cretin.[5,6] Since these simulations account for photon coupling throughout the system, we label this latter analysis "global".

The remainder of the paper will expand on the topics presented in this section. *Section 2* describes the theoretical elements of line broadening in more detail;

Section 3 examines the local analysis, including illustrating the behavior of the line profiles with respect to variation of the plasma properties and an application to an Alcator C-Mod experiment; *Section 4* examines the global analysis, including an illustration of line emission from a slab and further comparison with Alcator C-Mod MARFE data; while *Section 5* motivates future research into magnetically-broadened line profile calculations.

2 Theory

As a prelude to the application of magnetically-broadened line profiles we briefly present the theoretical elements of the line profile code Beline and discuss their validity. The relevant features of Beline are the inclusion of the effects of an external magnetic field of order to $1T$-10^4T and the assumption of hydrogenic emitters. While applications to tokamak fusion experiments are presented, these line profiles are also valid for other types of magnetized plasmas, such as stellarator plasmas and a few percent of the main sequence stars around spectral type B. This section will begin by discussing the approximations and assumptions used in Beline, highlighting aspects related to the external magnetic field, and will continue by outlining the theoretical components of the line profile.

2.1 Validity of Beline Approximations

Three independent approximations, related to the presence of an external magnetic field, are used in Beline: (1) charged particles follow linear trajectories in the neighborhood of a radiating atom, referred to as the straight line path (SLP) approximation, (2) the Lorentz electric field (LEF) is negligible; and, (3) the emitter fine structure (FS) is negligible.[7] Provided the Debye length (λ_D) is less than the Larmor radius (r_L), the perturbing charged particle will be well-described by a linear, rather than hyperbolic, trajectory as it passes by the radiating atom. For ions this condition is given by $B < 194\sqrt{n_{i,20}}$, where n_{20} indicates that the value is in units of $10^{20}\mathrm{m}^{-3}$ and B is given in units of Tesla; for electrons this condition is given by $B < 4.54\sqrt{n_{e,20}}$. Since number densities are of order $10^{20}\mathrm{m}^{-3}$ and $B \sim 6T$ in Alcator C-Mod, this approximation is strongly satisfied for ions but is marginal for electrons. So long as the LEF ($\vec{F_m} \sim \vec{v} \times \vec{B}$) is less than the quasi-static ion microfield ($F_0 \sim n_i^{2/3}$) it may be neglected. Finally, as long as first order Zeeman effect is greater than the emitter FS, the latter may be neglected ($\mu_B B > mc^2\alpha^4$).

Beline also treats ions in the quasi-static approximation and electrons by the impact approximation. The quasi-static ion approximation is valid provided
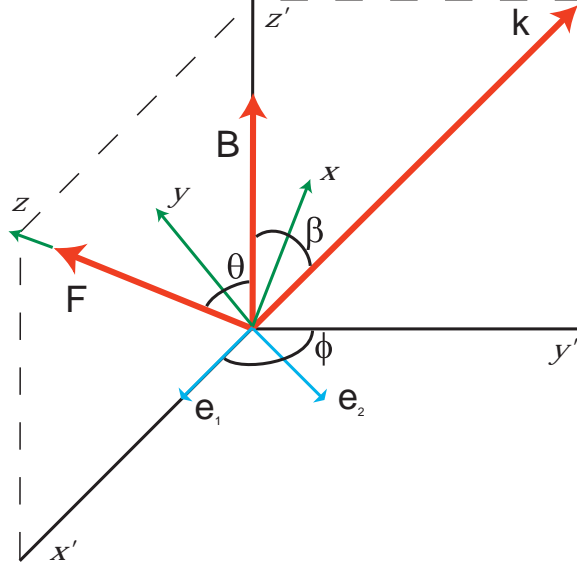
Fig. 1. Line Profile Geometry. This figure displays the $x'y'z'$ geometry used to calculate emitter energy levels and the xyz geometry used to calculate relative intensity in the dipole approximation. Also shown in this figure is the angle (β) between external magnetic field $(\vec{B})$ and emission direction $(\vec{k})$.

the full-width half-maximum (FWHM) of the normalized line profile in frequency space, $\Delta\omega_{1/2}$, is greater than the ion plasma frequency (ω_{pi}). The impact electron approximation will be valid provided $\Delta\omega_{1/2}$ is less than the electron plasma frequency (ω_{pe}). In the presence of a magnetic field these limits correspond to the case where $\vec{k}\|\vec{B}$ (see Fig. 1). When $\vec{k}\perp\vec{B}$ the cold plasma dispersion relation for electrons goes to the upper hybrid (UH) resonance frequency (ω_{UH}) and for ions goes to the lower hybrid (LH) resonance frequency (ω_{LH}). Since $\omega_{UH} > \omega_{pe}$ the former would increase the region of electron impact validity, while since $\omega_{LH} > \omega_{pi}$ the latter would decrease the region of static ion validity. This might encourage the use of an ion impact model, however Mathys has shown that a magnetic field lessens the discrepancies between static and impact profiles.[8] Ion impact broadening is important near line center, and in magnetically-broadened line profiles this effect tends to be obscured by Zeeman splitting.

2.2 Line Profile Components

For a given $\overline{n} \rightarrow n$ transition the total emission line profile is obtained by summing over component profiles and taking the average over microfield magnitude and direction. This may be written in general as:

$$\Phi_{\overline{n}n}(\omega) = \frac{1}{4\pi} \int P(F) \sum_{\overline{\nu}\nu} G_{\overline{\nu}\nu}(\vec{F})\phi_{\overline{\nu}\nu}(\omega, \vec{F})d\vec{F}, \tag{1}$$

4

where $P(F)$ is the quasi-static ion electric microfield distribution function, $G_{\overline{\nu}\nu}$ is the relative intensity of a $\overline{\nu} \rightarrow \nu$ component in the dipole approximation and $\phi_{\overline{\nu}\nu}$ is the profile of a $\overline{\nu} \rightarrow \nu$ component due to the influence of pressure broadening. Energy levels of a hydrogenic atom in both crossed electric ($\vec{F}$) and magnetic fields ($\vec{B}$) are determined from first-order perturbation theory.[9]

To elaborate on the terms above, for unpolarized radiation:

$$G_{\overline{\nu}\nu} = \frac{\omega_{\overline{n}n}}{n^2 f_{\overline{n}n}} \sum_{\rho=1,2} |\hat{e}_\rho \langle \nu | \vec{r} | \overline{\nu} \rangle|^2 , \tag{2}$$

where $\omega_{\overline{n}n}$ is the line center energy of the $\overline{n} \rightarrow n$ transition, $f_{\overline{n}n}$ is the total oscillator strength and $\hat{e}_\rho$ are the unit polarization vectors. $\hat{e}_1$ is taken to be perpendicular to the external magnetic field ($\vec{B}$) and emission direction ($\vec{k}$) plane, $\hat{e}_2$ is perpendicular to the $\hat{e}_1$-$\vec{k}$ plane (see Fig. 1). Profiles of $\overline{\nu} \rightarrow \nu$ transitions take into account the Maxwellian behavior of emitters (Doppler) and binary electron collisions:

$$\phi_{\overline{\nu}\nu} = \frac{1}{\sqrt{\phi} D_{\overline{\nu}\nu}} \int \psi_{\overline{\nu}\nu}(\omega - \omega_{\overline{\nu}\nu} - s, \vec{F}) \exp\left\{ -\left(\frac{s}{D_{\overline{\nu}\nu}}\right)^2 \right\} ds, \tag{3}$$

where $D_{\overline{\nu}\nu} = \omega_{\overline{n}n} \frac{v_{th,a}}{c}$ is the Doppler broadening parameter and $\psi_{\overline{\nu}\nu}$ is the electron profile. Various models can be used for the electron profile, including one based on the Bethe-Born approximation for the interaction between radiating atom and perturbing electron.

3   Local Analysis

Magnetically-broadened line profiles calculated by Beline depend on the polarization, magnetic field (B), angle of emission (β) relative to the magnetic field, electron density (n_e), electron temperature (T_e) and atomic (emitter) temperature (T_a). A discussion of hydrogenic emission line profile behavior is presented in the following subsection to motivate direct diagnostic applications. Comparisons between Beline line profiles and high-resolution D_α measurements from an Alcator C-Mod MARFE are made to illustrate a local analysis and at the same time verify the magnetically-broadened line profiles.

3.1   Behavior of Line Profiles

When an isolated hydrogenic atom is placed in an external magnetic field, it will possess an axis of symmetry which is aligned with the magnetic field. From
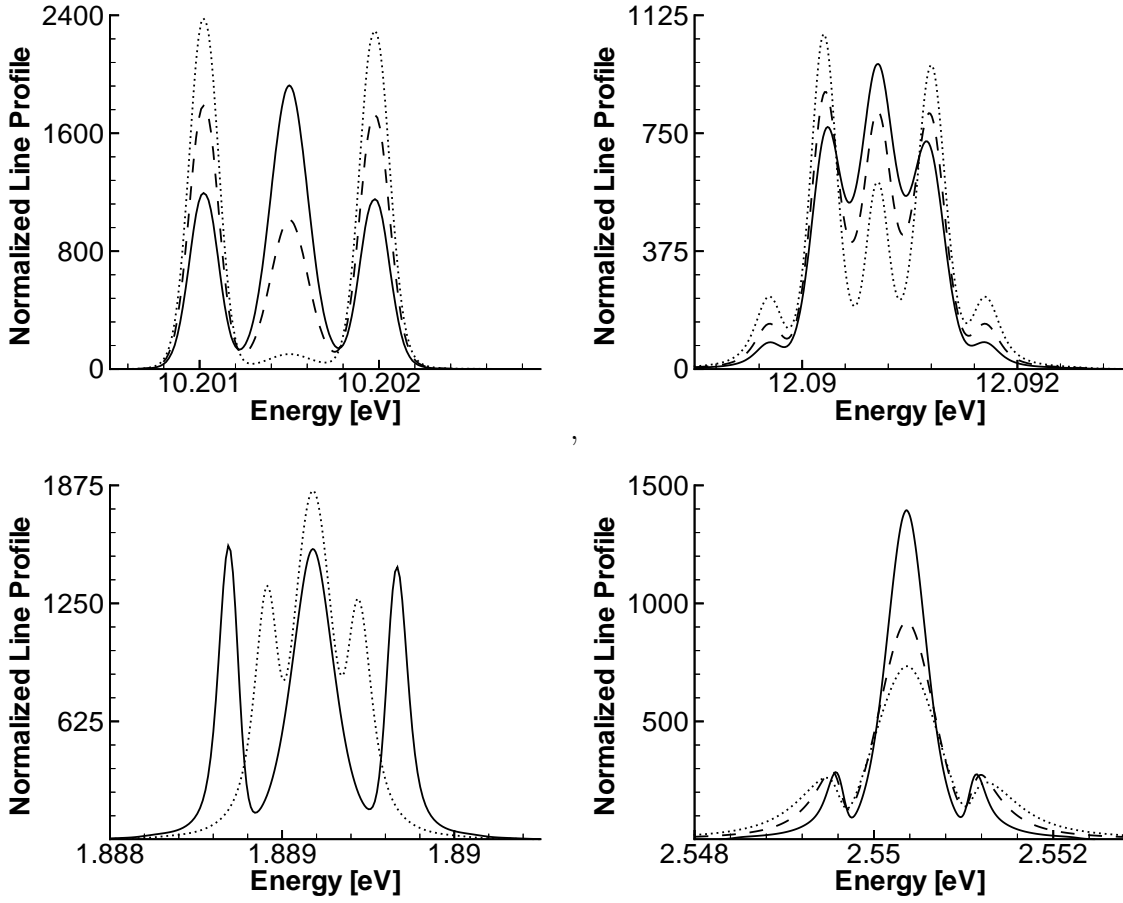
Fig. 2. a) (**upper left**) Deuterium Ly_α Lorentz Triplet. Dotted line corresponds to $\beta = 0$, dashed line to $\beta = \pi/4$ and solid line to $\beta = \pi/2$. Plasma conditions: $B = 8$T, $n_e = 10^{15}$cm^{-3} and $T_e = T_a = 0.1$eV. b) (**upper right**) Deuterium Ly_β line profile shows several transitions and the ion electric field influence on line strengths. Dotted line corresponds to $\beta = 0$, dashed line to $\beta = \pi/4$ and solid line to $\beta = \pi/2$. Same plasma conditions as (a). c) (**lower left**) Effect of increasing magnetic field strength on ΔE for D_α. Solid line corresponds to $B = 4$T and dotted line to $B = 8$T. For plasma conditions: $\beta = \pi/2$, $n_e = 10^{15}$cm^{-3} and $T_e = T_a = 1$eV. d) (**lower right**) Effect of increasing electron density on the D_β line profile. Solid line corresponds to $n_e = 50 \times 10^{13}$cm^{-3}, dashed line to $n_e = 100 \times 10^{13}$cm^{-3} and dotted line to $n_e = 150 \times 10^{13}$cm^{-3}. For plasma conditions: $\beta = \pi/2$, $B = 6$T and $T_e = T_a = 1$eV.

a classical viewpoint, light emitted parallel ($\beta = 0$) and perpendicular ($\beta = \pi/2$) to this axis of symmetry has properties dependent on polarization and oscillation energy, as may be seen in Fig. 2(a). Photons emitted perpendicular to the magnetic field are linearly polarized and display what is known as the Lorentz triplet, one central frequency (π-component) and two frequencies shifted up-down in energy (σ-components). Photons emitted parallel to the magnetic field are circularly polarized and show the absence of a π-component. This follows from classical electrodynamics; an oscillating particle does not radiate along its line of oscillation.

6

A closer examination of Fig. 2(a) reveals that the $\beta = 0$ line profile does have a small π-component. If we now consider the surrounding plasma, the ion microfield breaks the axial symmetry which existed for the isolated atom. For an atom in two arbitrary external fields, the energy levels are not degenerate and the line profiles possess $\overline{n}^2 n^2$ components, where $\overline{n}$ and n are the upper and lower principle quantum number (PQN) of a transition, respectively. Components beyond the Lorentz triplet are readily observable in Fig. 2(b).

For diagnostics it is interesting to study the line profile dependance on different system properties. In Alcator C-Mod the diagnostic view is perpendicular to the magnetic field, so we restrict our study to $\beta = \pi/2$. We further restrict our study to the optically-thin Balmer lines. The relative intensities of π- and σ-components in Figs. 2(c) and (d) are characteristic of transitions with different changes in PQN. Specifically, if the change in PQN ($\Delta n = \overline{n} - n$) is odd, as in Fig. 2(c), the π- and σ-component intensity are comparable; if Δn is even, as in Fig. 2(d), the π-component dominates.

The odd Δn D_α line presented in Fig. 2(c) shows two profiles differing in magnetic field strength (B) by a factor of 2. As B doubles, the difference between π- and σ-component peaks (ΔE) increases by nearly the same factor. In the absence of the microfield, the Zeeman effect would give $B = \Delta E/\mu_B$, where ΔE is the measured energy difference and $\mu_B = 5.78838 \times 10^{-5}$eV/T is the Bohr magneton. The linear relationship between the line splitting and B is modified by the ion electric microfield. For the 8T line profile in Fig. 2(c), $\Delta E = 4.9135 \times 10^{-4}$eV and $B = 8.489$T, and the Zeeman formula overestimates the true magnetic field strength by several percent.

While there is no simple formula for determining magnetic field strength from measurements of the energy difference between π- and σ-components, the magnetic field strength in the emission region may be determined by line profile modeling. Given the local plasma temperature and density, Beline may be used to find the magnetic field strength which matches the experimental ΔE. On Alcator C-Mod the plasma parameters are known (or measured) well enough for this to be a viable magnetic field strength diagnostic, as demonstrated in the next subsection.

The even Δn D_β line presented in Fig. 2(d) shows three profiles for differing electron densities, n_e. Two noticeable effects on the line profile are the broadening of the π-component and the increase in ΔE. The increase in ΔE with n_e is loosely referred to as the linear Stark effect and competes with the Zeeman effect in the D_α line profiles. Use of the increase in FWHM with n_e is a standard diagnostic for high-density plasmas. Here, the line width is also significantly affected by Doppler broadening and line profile modeling, rather than a simple analytic formula, must be used to determine electron density in even Δn lines.

Table 1
Time evolution of MARFE plasma properties.

Time [s]	$\langle \Delta E \rangle$ [eV]	$\langle n_e \rangle [\text{cm}^{-3}]$	$\langle T_e \rangle$ [eV]	B [T]	R [cm]
0.45	4.3×10^{-4}	0.95×10^{15}	0.94	7.02	47
0.50	4.1×10^{-4}	0.98×10^{15}	0.97	6.73	47
0.55	3.9×10^{-4}	0.88×10^{15}	0.93	6.44	47
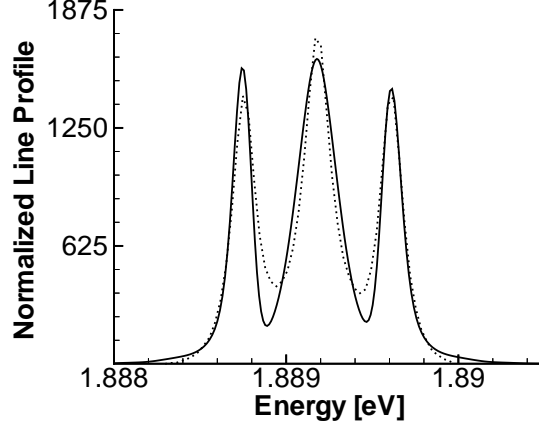
Fig. 3. Comparison between Alcator C-Mod MARFE D_α theoretical (solid line) and experimental (dotted line) line profiles at time $t = 0.5$s. The theoretical curve has not been instrumentally broadened.

3.2 Comparison with Experiment

To compare with experiment we perform a local analysis of D_α line radiation and determine the magnetic field strength in the emission region. The line profile modeling requires knowledge of electron density and temperature, where we assume $T_e \sim T_a$; β is determined by experimental alignment. There exist plasma diagnostics which measure n_e and T_e on Alcator C-Mod. We reduce sensitivity to these quantities by considering an experiment where they are held fixed while the magnetic field is varied in time. Such an experiment has been performed on Alcator C-Mod through formation of a midplane MARFE with ramping of the toroidal magnetic field ($B_{\phi 0}$) from 5.4T to 3.24T.

We discuss an Alcator C-Mod experiment where a MARFE formed near the inner wall $z = -12$cm. The local analysis procedure is as follows. ΔE is taken from experiment, various diagnostic data is averaged to estimate n_e and T_e, and then B is varied until the calculated profile agrees with measured ΔE. This procedure was followed for three different times, and hence for three different magnetic field strengths, during the Alcator C-Mod MARFE experiment. Table 1 summarizes the analysis and Fig. 3 shows a comparison between Beline and the experimental D_α line profiles at time $t = 0.50$s. Since the magnetic
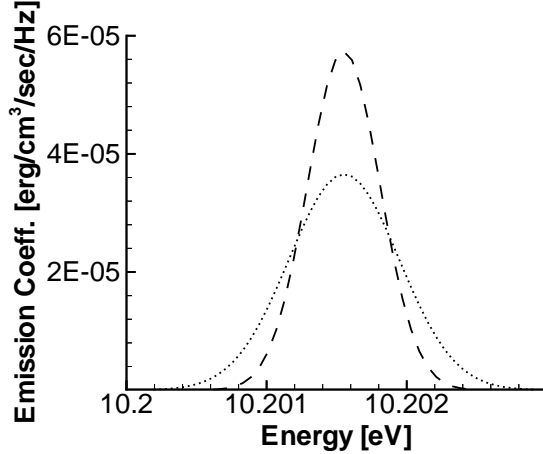
Fig. 4. Emission Coefficient for Ly_α. Including magnetic field effects (dotted line) nearly doubles the FWHM; dashed line does not include magnetic field effects.

field geometry is well known in Alcator C-Mod, it varies as the inverse of the major radius, once B is determined the emission location is also determined. Calculation of the emission location shows a stationary MARFE, consistent with CCD camera data.

There are discrepancies between the theoretical and experimental line profiles presented in Fig. 3. The experimental line profile shows a slight difference in the shift from line center to the red and blue σ-component peaks, while the theoretical line profile is symmetric about line center. The theoretical line profile shows an asymmetry between the peak intensities of the red and blue σ-components, while the experimental line profile does not. The theoretical asymmetry in peak intensities is attributable to the use of the electron impact approximation. This aspect of the model will be improved in future work.

4 Global Analysis

Computational modeling of plasma regions with optically-thick lines depends strongly on the line profiles. Inclusion of magnetic broadening can have a noticeable effect on radiation transport. This point will be demonstrated by comparing one-dimensional NLTE radiation transfer simulations with and without magnetic effects.

4.1 Finite and Semi-Infinite Slab Example

In order to quantify magnetic-line broadening effects on radiation transfer we use a simple semi-infinite slab with uniform plasma properties and study the
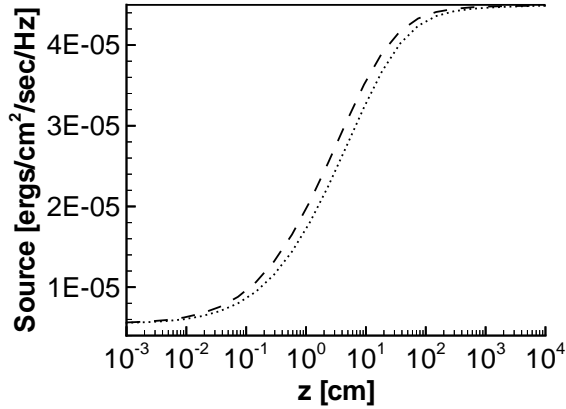
9

Fig. 5. Ly_α line center source function approach to black-body. Black-body (solid line), without magnetic field (dashed line) and with magnetic field (dotted line).

emergent intensity and the source function (S) of the slab. The source function is given by:

$$S(\tau) = \frac{2h\nu^3}{c^2} \frac{1}{\frac{n_l g_u}{n_u g_l} - 1} = (1 - \epsilon)\bar{J} + \epsilon B_\nu, \tag{4}$$

where n_u and n_l are the upper and lower excited state densities, respectively, with statistical weights g_u and g_l, $\bar{J}$ is the mean intensity, B_ν is the Planck function and ϵ it the probability that a line photon is destroyed by a collisional process. Thus, S directly reflects the distribution of excited state atoms and provides information about the internal radiation field.[10,11] The plasma conditions are: magnetic field $\vec{B} = (6\text{T})\hat{x}$ ($\beta = \pi/2$), Deuterium density $n_D = 10^{15}\text{cm}^{-3}$ and electron (ion) temperature $T = 1.2\text{eV}$. Line profiles calculated by Beline with and without a magnetic field are presented in Fig. 4. The profile in the absence of a magnetic field reduces to a standard Voigt function.

In the infinite optical depth limit, the source function and radiation intensity both approach the Planck function. Fig. 5 presents the approach of the source function to this limit, both with and without magnetic field effects. The magnetic field broadens the line profile, allowing photons to penetrate further into the slab before being absorbed and reemitted. Fig. 6 presents the radiation intensity emerging from a slab of finite thickness $T = 3.2\text{cm}$, which matches the thickness of the MARFE analysis presented in the next subsection. Integrating over the profile, the emergent brightness increases from 2.70×10^6 [ergs/cm^2/sec/ster] to 3.33×10^6 [ergs/cm^2/sec/ster] as the magnetic field is turned on, while the peak intensity decreases.
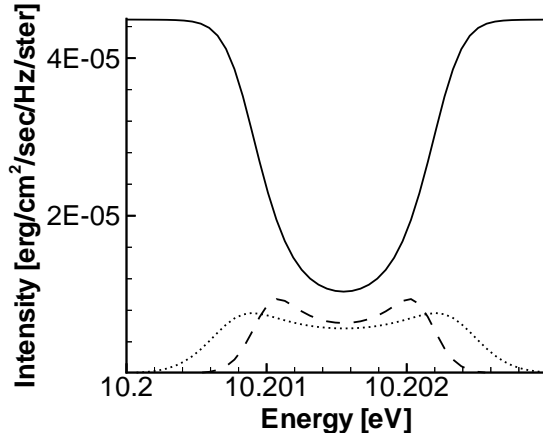
Fig. 6. Radiation intensity escaping finite atmosphere of thickness $T = 3.2$cm. Without magnetic field (dashed line) and with magnetic field (dotted line). Solid line is the intensity emerging from a semi-infinite slab without magnetic field effects.

4.2   Comparison with Experiment

To compare with experiment we return to the Alcator C-Mod MARFE used in *Local Analysis* and restrict ourselves to a single time $t = 0.50$s. This global analysis allows us to extend the local analysis from zero dimensions (cell) to one dimension (slab) and from optically-thin to optically-thick plasmas. The local D_α analysis showed that the MARFE is stationary, or in hydrodynamic equilibrium. Moreover, due to the short excited state lifetime, ~ 1 ns, the D_α emission, which is constant for 1 ms, should be in radiative equilibrium. These assumptions allow us to use fixed input plasma property profiles in the radiative transfer code Cretin to study magnetic broadening effects on radiation emerging from the plasma.

We are primarily interested in the emergent line radiation. Since we do not have a good theoretical or computational understanding of the MARFE, we make several assumptions about the plasma temperature and density profiles. This is consistent with our goal to demonstrate that magnetically-broadened line profiles are necessary for simulating the MARFE.

There are two distinct regions in the MARFE: a high-density, low-temperature radiating region and a low-density, higher-temperature region. This is consistent with previous theoretical work describing MARFE formation.[12] Justification for other profile features in Fig. 7 includes: width of radiating region ($L = 3.2$cm) is estimated from CCD camera observations; $T_e = T_i = T$ is assumed constant ($T = 1.2$eV) over domain of MARFE and then rapidly increases, $\sim R^4$, toward core plasma; $T = 1.2$eV optimizes emission from MARFE; ion density $n_i = 2.4 \times 10^{14}$cm^{-3} is taken as constant and set equal to an edge-core boundary value; magnetic field strength is standard and varies as
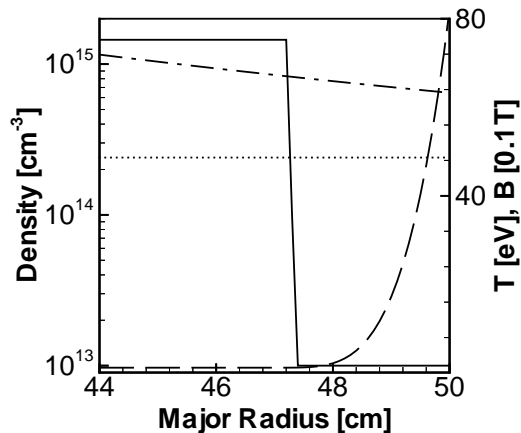
11

Fig. 7. Cretin input system property profiles used to simulate an Alcator C-Mod MARFE. Deuterium density (solid line), ion density (dotted line), temperature (dashed line) and magnetic field (dash-dot line).
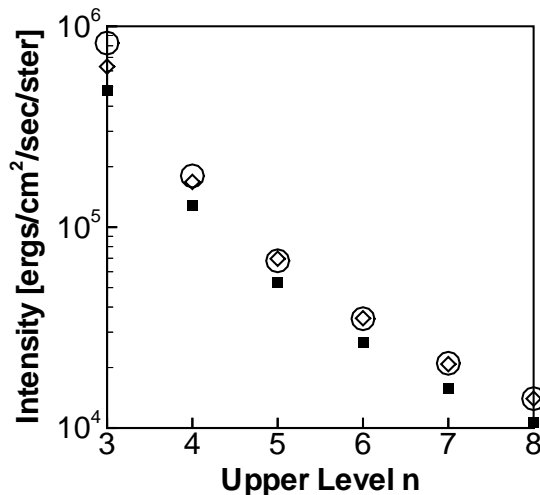

Fig. 8. Numerical and experimental Balmer series lines for and Alcator C-Mod MARFE. Experimental data (circle), Cretin without magnetic field effects (triangle) and Cretin using only Ly_α Beline line profiles (solid square).

$1/R$; the Deuterium density, which seeks to define radiating and non-radiating regions, has a value of $n_D = 10^{13} \text{cm}^{-3}$ outside of MARFE and a variable amount inside. The Deuterium density inside the MARFE was adjusted to match the upper level Balmer series lines since these are known to be optically thin and are not likely to be influenced by molecular contributions. As Fig. 8 shows, excellent agreement is obtained between simulation and experiment without magnetic field effects. Fig. 9 shows the final density profiles obtained by Cretin. The ionization fraction has increased drastically in the radiation region, with slight falloffs close to the radiating boundaries.

The Lyman series lines, up to upper level PQN of 6, are optically thick, and the
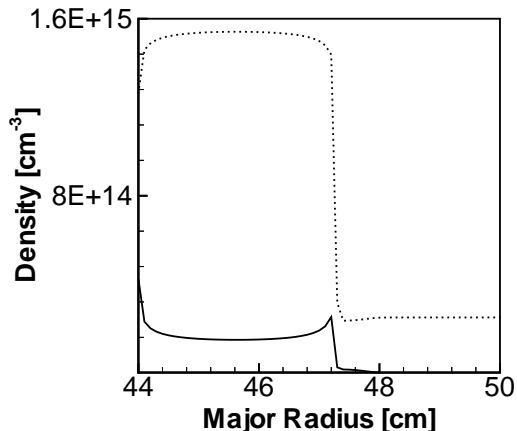
12

Fig. 9. Cretin final density profiles showing increased ionization away from the wall for the Alcator C-Mod MARFE simulation: Deuterium density (solid line) and ion density (dotted line).
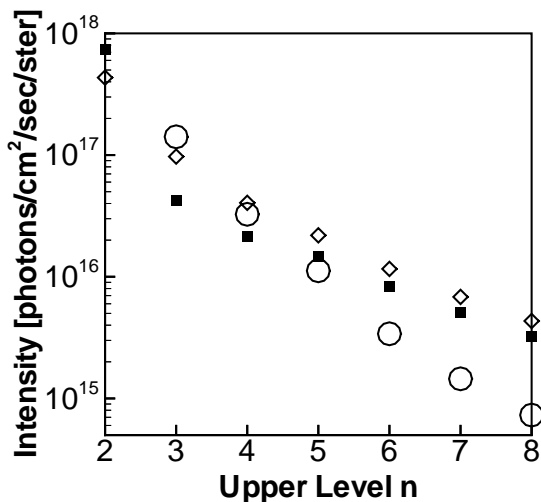

Fig. 10. Numerical and experimental Lyman series lines for and Alcator C-Mod MARFE. Experimental data (circle), Cretin without magnetic field effects (triangle) and Cretin using only Ly_{α} Beline line profiles (solid square).

Cretin simulation without magnetic field effects does not match experimental data (see Fig. 10). The intensity decreases much more quickly with PQN for experiment than simulation. When the magnetic field is included for the Ly_{α} line only (see solid squares in Fig. 10), the decrease in intensity from Ly_{α} to Ly_{β} becomes much steeper. It is quite plausible that extending the magnetic field effects to the other Lyman lines will improve the comparison with the experimental data for the first few lines since the relative effects should decrease for the lower opacity upper series lines. However, at the present time we have not included these effects for all the necessary lines. It is clear that including the magnetic field for a single line has a significant effect on the entire radiation spectrum, see the solid squares in Figs. 8 and 10. Other

13

interesting aspects of including magnetic field effects in the simulation include a 76 percent in increase in the opacity (as calculated from D_α/Ly_α) and a 70 percent increase in Ly_α brightness, which is about three times more than expected from our simple finite slab illustration.

5 Discussion

We have discussed the implementation of magnetic and electric field broadened lines and applied these to both local and global analysis. In a local analysis the line profiles were used to directly simulate emergent spectral features and hence quantified system properties for a well defined emission region. This computational analysis is valid provided the emission region is localized and the system is optically thin. In a global analysis, the magnetic field was found to have a significant effect on the emergent radiation in an optically thick plasma. Both analysis methods were applied to an Alcator C-Mod MARFE.

In the local analysis section (*Section 3*), optically-thin Balmer lines were studied to identify line profile features which depend directly on the plasma properties. Odd PQN transitions, e.g., D_α, are useful for determining magnetic field strength (B) and even PQN transitions, e.g., D_β, are useful for determining electron density. Comparison with experimental line profiles from the local D_α MARFE analysis indicated that one needs to explore the electron impact model used in the line profiles computation.

In the global analysis section (*Section 4*), optically-thick Lyman lines were studied to quantify magnetic effects on line radiation. In these plasmas, line radiation is strongly dependent on magnetically-broadened line profiles. Thus, our understanding of the flow of radiation energy, which is related to our understanding of the power balance in the plasma, is strongly depended on magnetically-broadened line profiles. Specifically, turning on magnetic effects for a single line (Ly_α) nearly doubled the amount of line radiation emerging from the system for that line. And turning on the magnetic field effects was seen to affect emerging radiation in all other lines.

Future work in this area will seek to improve the theoretical line broadening by removing or improving some of the approximations discussed in *Section 2* and extending the model to all elements. In addition, as this paper demonstrated that computational modeling of emission spectra is necessary for plasma diagnostic applications, numerical techniques and algorithm optimizations for magnetically-broadened line profile calculations will be investigated.

Acknowledgments

References

[1] Terry JL, Lipschultz B, Pigarov AYu, Krasheninnikov SI, LaBombard B, Lumma D, Ohkawa H, Pappas D, Umansky M. Phys Plasmas 1998;5:1759.

[2] Nikiforov AF, Novikov VG, Uvarov VB. Quantum Statistical Models of Hot Dense Matter and Methods for Computation Opacity and Equation of State. Moscow: Fizmatlit: Physics and Mathematics Publishers Company, Russian Academy of Science, 2000. [In Russian]

[3] D'yanchkov LG, Novikov VG, Nikiforov AF, Pigarov AYu, V.S. Vorob'ev VS. MIT PSFC 1999; PSFC/RR-99-9.

[4] Lipschultz B, LaBombard B, Marmar ES, Pickrell MM, Terry JL, Watterson R, Wolfe SM. Nuc Fusion 1984;24:977.

[5] Scott HA. JQSRT (this issue).

[6] Scott HA, Mayle R. Appl Phys B 1994;58:35.

[7] Hoe N, Grumberg J, Caby M, Leboucher E, Couland G. Phys Rev A 1981;24:438.

[8] Mathys G. Astron Astrophys 1984;141:248.

[9] Demkov YuN, Monozon BS, Ostrovskiĭ VN. Sov Phys JETP 1970;30:775.

[10] Avrett EH, Hummer DG. MNRAS 1965;130:295.

[11] Mihalas D. Stellar Atmospheres. San Francisco: W.H. Greeman and Company, 1978.

[12] Drake JF. Phys Fluids 1987;8:2429.